X-ray Optics for Synchrotron Radiation; Perfect Crystals, Mirrors and Multilayers

Michael Hart* and Lonny Berman

*National Synchrotron Light Source, Brookhaven National Laboratory, Upton, New York 11973, USA.
E-mail: mhart@bnl.gov*

Abstract

The X-ray optical properties of mirrors and Bragg reflecting perfect crystals are almost perfectly matched to the characteristics of synchrotron-radiation sources. That the X-ray refractive index is close to but less than one was realised early in the history of X-ray scattering – consequences are that mirrors exhibit total external reflection over a small angle range, *ca* 0.01 rad, and perfect crystals totally reflect X-rays in a small angle range, ∼ a few seconds of arc near the Bragg angle. The theory and application of these unique properties was developed in considerable detail in the three decades before the advent of the synchrotron-radiation era. This historical development is traced with special emphasis on the way in which the optical concepts were then straightforwardly applied to synchrotron-radiation X-ray optical design. In more recent times, the technology of synthetic multilayers has been developed so that these too are widely used in X-ray optics for synchrotron-radiation beamlines. As X-ray synchrotron-

---

Michael Hart is at present the Chairman of the National Synchrotron Light Source at Brookhaven National Laboratory. From 1975 to 1977, he was Special Advisor to the Central Policy Review Staff at the Cabinet Office, Whitehall, UK. From 1976 to 1984, he was Wheatstone Professor and Head of the Physics Department of King's College, London. He was Science Programme Coordinator for the SRS at the SERC Daresbury Laboratory from 1985 to 1988 and Professor of Physics at Manchester University from 1985 to 1993. His research interests are X-ray physics, especially X-ray optics.

Lonny Berman has been a physicist with the NSLS Experimental Systems Group since 1987. He built and is the Spokesperson for the X25 wiggler X-ray beamline. His research focuses on X-ray optics, X-ray scattering and photoemission. Lonny is the NSLS interface for the structural biology program at state of the art. He is also a member of the X24A beamline PRT, which addresses scientific applications of low-energy X-rays, and is a member of the X-ray optics development team for the new X13 undulator X-ray beamline.

radiation sources were born, perfect-crystal X-ray optics and crystal-growth technology matured; this symbiosis was not planned, it could not have been planned ... but it works, spectacularly!

1. Historical introduction

In the first volume of *Acta Crystallographica*, a paper by Ramachandran (1948) resolved a 30 year debate about the theories of Darwin (1914*a,b*), Ewald (1917) and Prins (Prins, 1930; Kohler, 1933); they had predicted three different results for the Bragg reflection curve from a perfect crystal. Ramachandran concluded that 'the Ewald and Darwin theories, although they follow very different mathematical methods, lead exactly to the same results when appropriate physical assumptions are made' and that 'the dynamical theory also gives Prins's formula for an absorbing crystal'. Until the late 1950s when ideally perfect crystals became almost routinely available, experiment and theory of X-ray diffraction made only spasmodic progress.

W. C. Röntgen, in his third Communication, dated March 1897, stated 'Ever since I began working with X-rays, I have repeatedly sought to obtain diffraction with these rays: .... The experiments on the permiability (for X-rays) of plates of constant thickness cut from the same crystal in different orientations, which were mentioned in my first Communication, were continued. Plates were cut from calcite, quartz, tourmaline, beryl, aragonite and barytes. Again no influence of the orientation on the transparency could be found.' Following the discovery of X-ray diffraction by crystals in 1912, it became clear that the effect had been predicted in Ewald's 1912 thesis (Ewald, 1950). Within 3 years, it was also known that neither Ewald's nor Darwin's (1914*a,b*) theories of diffraction by perfect crystals actually predicted the observed intensities. Bragg (1914, 1915) noted that some diamond and some calcite crystals diffracted intensities proportional to the structure amplitude but that all others so far studied behaved as 'mosaic crystals', a term invented by Darwin early on to account for the higher-than-expected intensities that were usually observed. In most crystals, the diffracted intensity agreed with Darwin's formulae for the mosaic crystal wherein the difracted intensity is

proportional to the square of the structure amplitude. And so the situation remained for a very long time. Most crystals seemed to follow the ideally mosaic paradigm, but low intensity due to extinction was frequently observed (and largely ignored!), and a few crystals approached agreement with the Ewald/Darwin intensity predictions.

Of these, calcite became of utmost importance as a unique monochromator in spectroscopic experiments. By 1922, Davis & Stemple (1921, 1922) had obtained high-resolution calcite crystals that gave an instrument profile under Bragg reflection only 18″ wide in the newly invented double-crystal spectrometer. Within a few years, this had been reduced to about 6″ in agreement with the perfect-crystal theories. Ehrenberg & Mark in 1927 found diamonds with 111 reflection curves only 4″ wide. Thus, the Darwin–Prins curve and its width had been verified *in two crystal species*. The first high-quality synthetic single crystals were of rock salt, NaCl, grown from the melt. They were investigated by Renninger in 1934. Crystals a few square mm in area gave double-crystal widths as small as 7.1″ in the 200 Bragg reflection, much lower than any previously observed for rock salt, and both the integrated reflectivity and the diffraction width were close to the values predicted by perfect-crystal diffraction theory. The state of development and confidence in the perfect-crystal dynamical diffraction theory is well described in detailed measurements and calculations for rock salt by Renninger (1934) and for calcite by Compton (1934).

The structure and properties of wavefields inside periodic media, such as crystals, during Bragg reflection are finely detailed and subtle. In appropriate circumstances, large and surprising intensity changes may be observed. Borrmann (1941, 1950) first observed that thick quartz crystals became anomalously transparent when oriented near the Bragg position. The effect can be very large; an intensity change from detector background to many thousands of counts per second with laboratory X-ray tubes (Cu $K\alpha$) and modern crystals of germanium or silicon. The observation was quickly verified by Campbell (1951), Schwarz & Rogosa (1954) and Brogren & Adell (1954), and shown to be quite consistent with and quantitatively predicted by the then established dynamical diffraction theory (von Laue, 1949; Hirsch, 1952; Zachariasen, 1945). Knowles (1956), at the suggestion of Ewald, sought to detect the anomalous transparency effect in monochromatic neutron diffraction from $3CdSO_4 \cdot 8H_2O$ but failed to find a convincing effect because the available crystals were not sufficiently perfect. He also studied calcite and searched for the $^{40}Ca(n\gamma)^{41}Ca$ neutron capture γ ray at 1.93 MeV as the crystal was rocked through the 211 Bragg reflection for 1.30 Å neutrons obtained from a calcite monochromator in the parallel setting. Theory and experiment were in perfect agreement and for the first time the microscopic standing wavefield was 'seen'

experimentally (see Knowles, 1956, Fig. 7). The equivalent X-ray experiment was demonstrated by Batterman (1962) who monitored the germanium fluorescence signal as a germanium crystal was rocked through the Bragg position with Mo $K\alpha$ radiation.

2. Theoretical background and laboratory experiments before the synchrotron-radiation era

The first observation of terrestrial synchrotron radiation and the invention of the transistor occurred within a year or so of the foundation of *Acta Crystallographica*. Although X-ray synchrotron-radiation sources were not used for experiments until much later, almost perfect germanium crystals became available and led to a wide range of diffraction experiments aimed at both the fundamentals of dynamical diffraction and to delineate and understand the crystal defects, their formation and propagation. By 1960, almost perfect silicon crystals also became available. Most recently, in the 1990s, a few large synthetic diamonds have been produced and used as optical elements in high-power synchrotron-radiation beamlines.

The principal phenomenon that distinguishes dynamical diffraction from kinematical diffraction is the effect of extinction. This results from the depletion or re-direction of the bulk of the incident X-ray intensity during Bragg reflection because of the diffraction effect itself. Consequently, the scattering events in different parts of the illuminated crystal are correlated. Under kinematical diffraction, the diffraction process is relatively weak such that scattering events in different parts of the exposed crystal are uncorrelated. This is usually the case when the scattering power of the Bragg reflection is intrinsically weak or when the crystal is mosaic or imperfect. Here, the dominant factors responsible for depletion of the incident X-ray intensity are the size of the crystal and X-ray absorption.

Among the predictions of dynamical diffraction theory is the presence, within the crystal, of X-ray standing wavefields during Bragg reflection, whose nodes and antinodes are in or out of registry with the Bragg planes. These are simply Bloch-type eigensolutions of Maxwell's equations governing the propagation of electromagnetic radiation inside a medium of periodic dielectric constant. Their existence was predicted by von Laue in 1935, who later invoked them (von Laue, 1949) to explain anomalous X-ray transmission accompanying Bragg diffraction in a perfect crystal (Borrmann, 1941, 1950). Confining our attention to the Bragg diffraction geometry, in which the diffracted X-ray beam exits the crystal *via* the same surface upon which the primary beam is incident, it can be shown that there exists a continuous transition from the excitation of one kind of standing wave field (with nodes degenerate with the Bragg planes) to the other kind (with nodes centered between the Bragg planes) as the incidence angle (or

Table 1. *Representative diffracted bandwidths* $\Delta E/E$

hkl	Diamond	Silicon	Germanium
111	5.8×10^{-5}	1.3×10^{-4}	3.2×10^{-4}
220	2.0×10^{-5}	5.6×10^{-5}	1.5×10^{-4}
311	9.0×10^{-6}	2.7×10^{-5}	6.9×10^{-5}
400	8.0×10^{-6}	2.3×10^{-5}	6.1×10^{-5}

X-ray wavelength) is scanned through the reflection. Within the range of Bragg reflection, referred to as the Darwin (1914*a,b*) width, there is essentially unit reflectivity. The ratio of diffracted to incident electric field amplitudes is

$$E_H/E_0 = -|b|^{1/2}(|P|/P)(F_H/F_{\bar{H}})^{1/2}[\eta \pm (\eta^2 - 1)^{1/2}]. \tag{1}$$

The 'reduced-angle' parameter η is a coordinate consisting of the sum of a term proportional to the incidence-angle deviation from the nominal Bragg angle and a term proportional to the shift in Bragg angle arising from the refractive index inside the crystal. The factor b relates to the asymmetry of the Bragg reflection, *i.e.* the angle between the Bragg and surface planes projected into the plane of X-ray scattering, and is -1 for a symmetric reflection. The range of Bragg reflection occurs in the region where the magnitude of η is less or equal to 1. P is the polarization factor, 1 for sigma (σ) and $\cos 2\theta_B$ for pi (π) polarization. F_H is the structure factor for the H Bragg reflection and consists of the Fourier summation of the atomic scattering form factors within the unit cell (including the anomalous-dispersion corrections) weighted by the Debye–Waller contributions of individual scatterers. The diffracted-to-incident-beam intensity ratio is simply the square of the modulus of the electric field amplitude ratio, and the Darwin angular width of total reflection for a symmetric reflection is

$$\Delta\theta_D = 2r_e\lambda^2|P||F_H F_{\bar{H}}|^{1/2}/\pi V \sin 2\theta_B. \tag{2}$$

Here, r_e is the classical electron radius (2.82×10^{-15} m), λ is the X-ray wavelength, V is the unit-cell volume and θ_B is the nominal Bragg angle. It is important to note that all of the X-ray physics describing Bragg reflection in perfect crystals is contained in equation (1). This, together with the boundary conditions on the electromagnetic field and Snell's law determines completely the excitation of wavefields within the crystal. The polarization factor P takes one of two values for linearly polarized incident radiation and the reduced angle parameter term has two values corresponding to the $+$ and $-$ signs in the term in brackets. Thus, for a linearly polarized (or unpolarized) incident wave, there are four waves in the crystal – in terms of classical optics all crystals are doubly birefringent and doubly dichroic near the Bragg angle. Note that F_H is complex both by virtue of optical dispersion and because of the phase shifts between different atoms in the unit cell. We

anticipate that all of the known effects in classical optics will be observed in Bragg reflecting crystals but with *twice the number of parameters per Bragg reflection*!

In classical optics where the length scale of materials structures is small compared to the wavelength of light, materials are only isotropic, uniaxial or biaxial. The optical indicatrix is an ellipsoid. In the X-ray case, the indicatrix is a sphere but the sphere is split into a four-branched (or multiply branched) surface whenever Bragg reflection occurs. The overall effect is that for each energy the Kossel diagram (see James, 1948) is a representation of the refractive index as a function of orientation.

The most important performance parameter for perfect-crystal X-ray monochromators is the reflectivity shown in Fig. (1*a*). It is very close to unity within the Darwin width. Since the photon beam emerging from a synchrotron source is linearly polarized in the synchrotron orbit plane, it is clear that the preferable scattering geometry for a monochromator is σ, *i.e.* perpendicular to the orbit plane (and thereby generally vertical at storage-ring sources). This orientation maximizes the delivered monochromatic photons for all possible X-ray wavelengths and simultaneously serves to enhance the beam polarization. The delivered photon flux is proportional to the Darwin width, which, for synchrotron optics applications, is more conveniently expressed in terms of the relative energy bandwidth for the H Bragg reflection:

$$\Delta E/E = \cot \theta_B \Delta\theta_D. \tag{3}$$

Through algebraic manipulation, this can be expressed as

$$\Delta E/E = 4r_e d^2|P||F_H F_{\bar{H}}|^{1/2}/\pi V, \tag{4}$$

where d is the d spacing of the Bragg planes. Table 1 gives relative diffracted bandwidths (for the σ-polarization geometry) for low-index Bragg reflections for diamond, silicon and germanium. Improved energy resolutions are attained for smaller d spacings as well as for smaller structure factors at the expense of diffracted flux. In practice, the intrinsic resolution of the crystal may be increased by the angular divergence of the incident X-ray beam.

The presence of the $|P|$ polarization term in equation (4) indicates that the energy bandwidth depends on the polarization state; we have listed in Table 1 the widths for the σ state which corresponds to dispersion in the vertical plane at bending-magnet beamlines. The narrower bandwidths of the higher-order Bragg reflections are truly realised at third-generation sources, because those sources have very low divergence in the vertical plane of diffraction.

All the waves excited inside the crystal are phase coherent, as they are in the optical case. Their relative phases are therefore important parameters which are shown in Fig. 1(*b*). Notice that the phase of the

diffracted wave with respect to the incident wave is $\pi/2$ for both polarization states at the center of the Bragg range, and that they both asymptotically tend to π on the low-angle side of the Bragg reflection range and to 0 on the high-angle side. Inside the crystal, the phase difference between the differently polarized waves is important and is also plotted in Fig. 1(b) (as a chain-dashed line). Two features of this are important: within the Bragg range the phase difference varies almost linearly as the angle is changed [from a minimum of about $-\pi/4$ for the case presented in Fig. 1(b) to a maximum of about $+\pi/4$] and outside the Bragg range the phase difference tends asymptotically to 0 at large angles. This is of importance for the performance of crystal-based

circular X-ray polarizers, as discussed in the next section.

Because the X-ray reflectivity approaches unity in the range of Bragg reflection, the penetration depth is limited by both extinction and absorption. In practice, extinction dominates as shown in Figs. 1(c), (d). The maximum extinction coefficient for the silicon 220 reflection is 365 mm^{-1} whereas the absorption coefficient is only 15 mm^{-1}. In optical terms, the difference in peak attenuation between the two linear polarization states is a manifestation of linear dichroism. The extinction effect is more dramatic in Fig. 1(d), which shows a penetration depth of only 1.1 µm inside the range of total reflection and anomalous transparency on
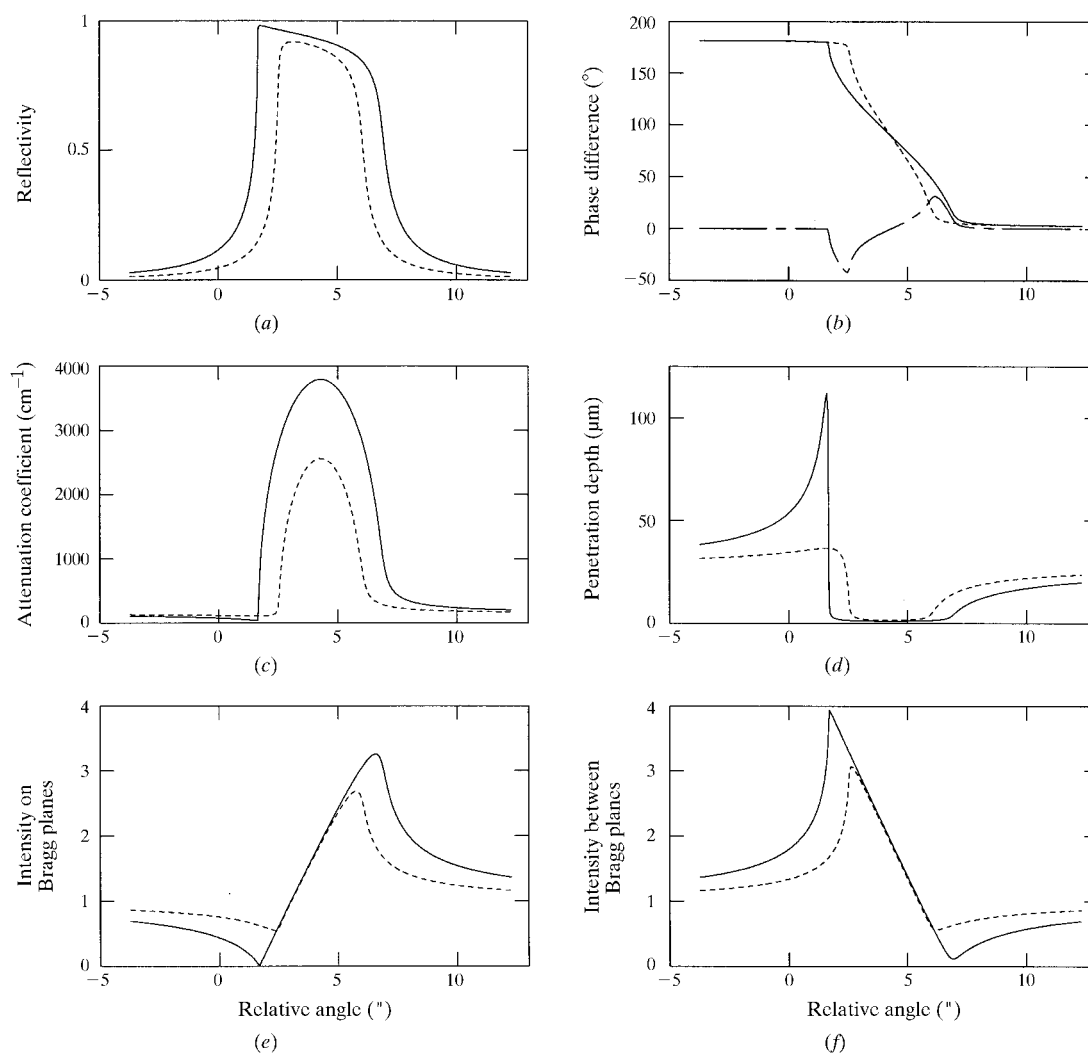

Fig. 1. Properties of X-ray wavefields calculated from equation (1) are plotted as a function of angle, proportional to η, for a symmetric Si(220) Bragg reflection at 8 keV photon energy, and for the σ (solid curves) and π (dashed curves) polarization geometries. (a) The X-ray reflectivity. (b) The phase difference of diffracted to incident electric field amplitudes. The difference of phase shifts between the two beam polarizations is shown as a chain-dashed line. (c) The attenuation coefficient of the X-ray beam inside the crystal. (d) The effective penetration depth of the beam below the surface. (e) The normalized electric field intensity on the Bragg planes and near the surface. (f) The normalized intensity midway between the planes. Away from the Bragg reflection, the attenuation coefficient and penetration depth are determined by photoelectric absorption and the electric field intensities are normalized to unity.

the low-angle side of the Bragg range. This last effect is the Bragg (reflection) case manifestation of the (transmission) Borrmann effect.

Pairs of waves inside the crystal create standing wavefields with spacings equal to d, the Bragg crystal spacing, and *Pendellösung* wavefields with spacings proportional to $\Delta\theta_D^{-1}$ [equation (2)]. The first pairing is responsible for manifestations of anomalous absorption such as the Borrmann effect. Their field intensities on the Bragg planes are shown in Fig. 1(*e*) and between the Bragg planes in Fig. 1(*f*). The second pair of waves represents birefringence which is crucial in polarizing X-ray optics.

Finally, Fig. 2 shows the relationship between the members of the harmonic series of 220, 440 and 660 Bragg reflections which are simultaneously present when a white beam of X-rays is diffracted by a perfect crystal. Clearly, such a beam is not ideally suited for either diffraction or spectroscopic experiments and designs for synchrotron-radiation beamlines must address that problem.

3. Applications of dynamical diffraction principles in synchrotron X-ray optics

3.1. *Perfect crystals*

Multiple-crystal or multiple reflection channel-cut crystal monochromators are employed to exploit these effects, for attaining high resolution, polarization control, divergence control and for harmonic rejection. Since the simultaneous higher-order Bragg reflections have narrower Darwin widths (see Fig. 2), offset multiple reflections can be used effectively for harmonic rejection (Hart & Rodrigues, 1978; Bonse *et al.*, 1983). Parallel alignment of successive crystal Bragg reflections can suppress the tails of the reflectivity curve while largely preserving the central region of peak reflectivity (Bonse & Hart, 1965). By slightly offsetting successive
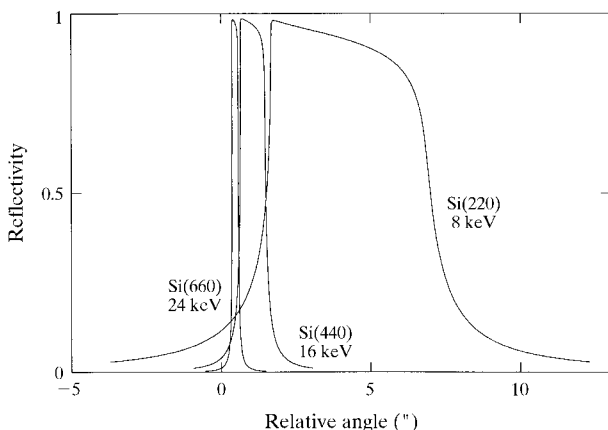

Fig. 2. Reflectivity for the 220, 440, 660 harmonic series in silicon at 8, 16 and 24 keV.

Bragg reflections from parallel alignment, the central region of peak reflectivity can be narrowed in angle (and in energy) considerably (Hart *et al.*, 1984; Berman *et al.*, 1985). The offset Bragg reflection scheme also provides tuneable linear X-ray polarizers (Hart & Rodrigues, 1979).

Linear X-ray polarizers were originally based on 90° Bragg scattering for which $\cos 2\theta$ is zero (Chandrasekaran, 1959; Cole *et al.*, 1961; Skalicky & Malgrange, 1972; Hart, 1978). Tuneable linear polarizers based on the Borrmann effect were used by Cole *et al.* (1961). Tuneable linear polarizers with exceptional extinction were first used by Hart & Rodrigues (1979) in the Bragg case of reflection.

A wide variety of circular X-ray polarizers, quarter- and half-wave plates, has been developed. It suffices here to list the aspects of dynamical theory that are exploited. In the Laue case (transmission), the *Pendellösung* interference effect has been exploited (Skalicky & Malgrange, 1972; Hart, 1978). Bragg-case transmission, in the tails of the reflection peak using the forward-diffracted beam, provides circularly polarized X-rays (Belyakov & Dmitrienko, 1991; Hirano *et al.*, 1991). Bragg–Bragg (Batterman, 1992) and Bragg–Laue (Mills, 1987) double reflections have also been used to create circularly polarized X-ray beams. A switching left–right circular polarizer has been demonstrated by Hirano *et al.* (1992).

Experimental applications requiring very high energy resolution, such as inelastic X-ray scattering and studies of Mössbauer systems, have taken advantage of high-index Bragg planes (*i.e.* small d spacing) and especially back-reflection conditions (for which the Darwin width broadens considerably in angle but minimizes in energy) for crystal monochromators and analyzers alike (Kohra & Matsushita, 1972; Brümmer *et al.*, 1979; Caticha & Caticha-Ellis, 1982; Graeff & Materlik, 1982). Dispersive multiple-reflection monochromators for Mössbauer applications (Siddons *et al.*, 1989; Ishikawa *et al.*, 1992) and large-collection-angle back-reflection crystal analyzers for inelastic scattering applications (Dorner *et al.*, 1986; Stojanoff *et al.*, 1992), are based on these principles.

There are many reviews of hard X-ray optics applied to synchrotron-radiation beamlines: Matsushita & Hashizume's (1983) review is particularly comprehensive.

3.2. *X-ray multilayers*

Fine monochromatic beam resolution is often unnecessary for many experimental applications of synchrotron radiation, and in such cases entails inefficient utilization of the continuous radiation spectrum. Broader bandwidth diffractive optics such as layered synthetic microstructures or multilayers, consisting of a periodic film of alternating heavy and light layers grown

Table 2. *Critical angles at 50% reflectivity for several mirror materials at 10 keV*

	Silicon	Silica	Copper	Gold	Platinum
θ_c (°)	0.1817	0.1812	0.3149	0.4407	0.4623
θ_c (rad)	3.17×10^{-3}	3.16×10^{-3}	5.50×10^{-3}	7.69×10^{-3}	8.07×10^{-3}

atop a substrate, can be designed to diffract photon-energy bandwidths that are 100 times broader than routinely diffracted by conventional crystal monochromators, resulting in a 'monochromatic' beam that is thereby that much more intense. Dynamical theory well explains the diffraction properties of multilayers (Underwood & Barbee, 1981). Multilayer combinations of W/Si, W/B$_4$C, Mo/Si, Mo/B$_4$C and others are available commercially. They are generally fabricated with bilayer spacings of 20–30 Å, with a total of >100 bilayers grown on silicon or glass substrates. These d spacings are about ten times bigger than for commonly used Bragg planes of Si or Ge monochromator crystals; it is therefore evident, from equation (4), that the sensitivity of the relative diffracted bandwidth to the d spacing is a major factor in explaining the broad bandwidth properties of multilayers. F_H/V is essentially the effective electron scattering density, which is similar for crystals and multilayers composed of the same elements. Multilayer monochromators are in common use at synchrotron sources; the current state-of-the-art is described by Ziegler (1995).

3.3. *X-ray mirrors*

Röntgen and many others spent much time trying to observe X-ray refraction, an effect predicted with confidence, especially after the discovery of X-ray diffraction. During the 1930s, definitive measurements of the critical angle below which total external reflection occurred, according to Snell's law for the case when the refractive index is less than one, were finally made (see, for example, Compton, 1934; James, 1948).

The complex refractive index in the X-ray energy range can be written in terms of the X-ray scattering amplitudes as

$$n = 1 - \alpha - i\beta. \qquad (5)$$

The critical angle of grazing incidence θ_c below which total external reflection occurs is given by

$$\cos^2 \theta_c = 2\alpha \qquad (6)$$

or

$$\theta_c = 0.00234\lambda(\rho Z/M)^{1/2}. \qquad (7)$$

Some values are given in Tables 2 and 3 for several materials that are commonly used for X-ray mirrors.

Since the maximum aperture of the mirror cannot exceed θ_c, there is a strong incentive to make mirrors with heavy elements so as to maximize the critical angle. Unfortunately, most of the materials that can be worked to the necessary figure are composed of light elements or have a low density – for example, copper, silicon, silicon carbide, silica and various glasses. The solution is to coat the mirror with a heavy element since the skin depth for the evanescent mode which enables total external reflection is only 100 Å or so at most energies of interest. Fig. 3(*b*) shows that a silicon mirror coated with just 500 Å of platinum would act as though it was a solid platinum mirror from the X-ray optical viewpoint. The thermomechanical properties of silicon combine with the X-ray optical constants of platinum to form an optimized mirror.

In practice, the surface roughness is a crucially important factor in mirror fabrication; only very recently have almost perfect X-ray mirrors become available. Over the last few years, approximately half of all X-ray mirrors have been manufactured from single-crystal silicon with thin metallic coatings.

4. Applications to synchrotron-radiation beamlines

Beamline X-ray optical systems fall generally into two classes: generic general-purpose beamlines that conform to a common design; and special-purpose beamlines designed for particular tasks. Since perfect crystals and
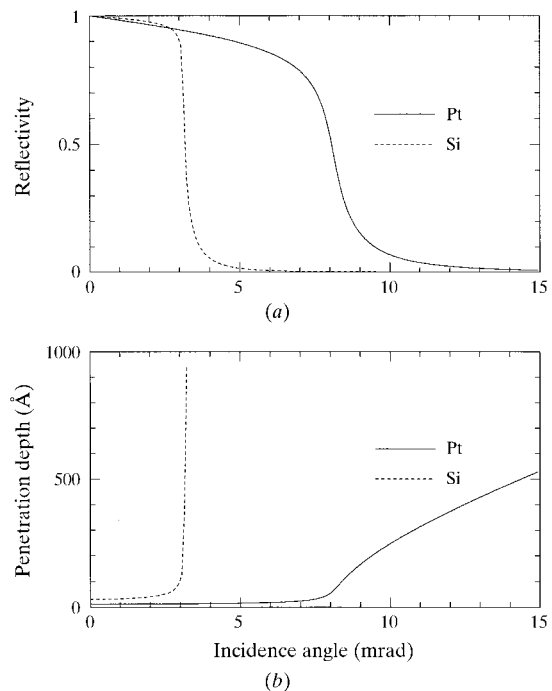

Fig. 3. Reflectivity of a silicon and platinum mirror at 10 keV X-ray energy and the corresponding beam penetration depth.

Table 3. *Critical angle for silicon at various X-ray energies*

	10 keV	15 keV	20 keV	25 keV	30 keV
θ_c (°)	0.1817	0.1211	0.0909	0.0727	0.0606
θ_c (rad)	3.17×10^{-3}	2.11×10^{-3}	1.59×10^{-3}	1.27×10^{-3}	1.06×10^{-3}

almost perfect mirrors have become available, the concepts and results of many years of experience of dynamical diffraction can be routinely invoked in beamline design. Most of the synchrotron-radiation facilities in the world publish their portfolio of beamlines, designs and functions (see, for example, http://www.nsls.bnl.gov/BeamLine/BeamLMenu.html and http://www.nsls.bnl.gov/Intro/AllSynch.html). For illustrative purposes, Fig. 4 shows a simple generic beamline that directs a tuneable, monochromatic, focused X-ray beam onto a sample.

In this simple example, the 'point' source is imaged onto the sample by a toroidal mirror. The doubly reflecting monochromator crystal, which may be a monolithic channel-cut crystal or two separate crystals, provides an undeviated tuneable monchromatic beam. In principle, subtle differences in performance arise if the crystal and mirror are interchanged. The horizontal aperture of the mirror is limited to twice the critical angle. Larger apertures can be achieved by using a sagittally focusing crystal monochromator instead (Sparks *et al.*, 1980). Harmonic rejection is achievable either by off-setting the parallelism of the two crystals or by using the energy dependence of the mirror critical angle. Of course, the beam could be used for spectroscopy, diffraction or small-angle scattering.

In practice, there are many variables that can dictate beamline design. For example, the sample may be in the form of a capillary or a sheet of material. Plane-wave beams may be necessary for high-angle or energy-resolution measurements. Polarization modulation or control may dominate the design requirements. In addition to the www references above, the tri-annual Synchrotron Radiation Instrumentation meetings (SRI'91, 1992; SRI'94, 1995; SRI'97, 1998) contain wide-ranging design information.

5. High-power X-ray optics

In modern storage rings, the thermal power in the photon beam can be a cause of temperature changes and inhomogeneity in the monochromator itself. Mirrors too may suffer sufficiently large heat loads to compromise their optical performance. Sample calculations show that the total photon power produced by wigglers can be in the kW range while undulators and focused white-radiation beams from bending magnets and wigglers can result in power densities in the 100 W mm^{-2} range. Bearing in mind that the surface figure of mirrors is critical to their performance and that the preservation of perfection and homogeneity in crystals is crucial to

delivering the Darwin efficiency, it is clear that the thermal response of these optical components is very important in practice.

Two simple thermal calculations suffice to illustrate the problems that arise in high-power X-ray beams. The important parameters that define the dynamic thermal response to changing beam current are beyond the scope of this summary.

5.1. One-dimensional heat flow

The steady-state thermal diffusion equation can be solved exactly in this case. With a power input Q/A per unit area, we require that

$$Q/A = k\nabla T = k(T_H - T_C)/t, \qquad (8)$$

where T_H, T_C are the hot and cold temperatures and t is the crystal or mirror thickness. In either case, a parallel plate becomes spherically bent to a radius R which is given by $R = t/\alpha(T_H - T_C)$. The resulting curvature is independent of the thickness of the material since we can combine these last two results to give $Q/A = k/\alpha R$. In the dynamical diffraction regime, sensitivity to curvature is extremely high, for example 1 km bend radii are easily detected. With $R = 1$ km in silicon (for which $k = 160$ W mK^{-1} and $\alpha = 2.33 \times 10^{-6}$), we find $Q/A = 68$ mW mm^{-2}; very low power density indeed compared to that routinely available at modern synchrotron-radiation sources, typically 100 W mm^{-2} on undulator beamlines.

5.2. Three-dimensional heat flow with cylindrical symmetry

The beam that emerges from the storage-ring dipole magnets and from most wigglers is a horizontal swath of radiation. From the thermal viewpoint, the footprint of these beams is therefore a line source of heat on a wafer or more particularly a semi-infinite conducting medium. In this case too, the thermal diffusion equation has
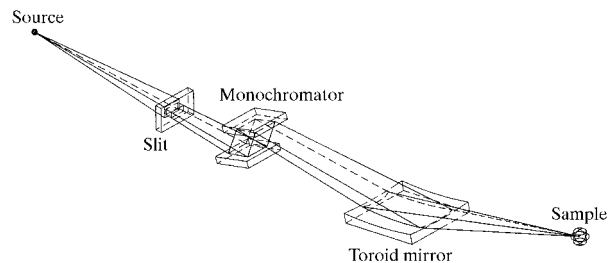

Fig. 4. Typical tuneable monochromatic focused beamline.

simple analytical solutions. The steady-state solution in cylindrical polar coordinates is

$$Q/L = 2\pi k(T_H - T_C)/\ln(R/r), \qquad (9)$$

where Q/L is the heat input per unit length. The important part of the solution is the $\ln R$ dependence of the heat loading on the distance to the distant cylindrical boundary at which the cooling heat sink is provided. For the case $R \gg r$, this result is exactly the same as the one-dimensional result, as expected. If $R = 0.1$ m, corresponding to a thick single-crystal block, then the hot beam footprint reaches the melting point of silicon when the heat flux exceeds 270 W mm^{-1} of input thermal power if the cold boundary is at room temperature. Such linear power densities are frequently encountered at synchrotron-radiation sources.

6. Choice of materials for monochromators and mirrors

At the highest thermal beam powers encountered, there are clearly problems at room temperature with silicon monochromators and with normal mirror materials from the point of view of X-ray optical performance.

In the case of mirrors, the mechanical properties of the mirror material can be chosen almost independently of the optical properties of the mirror surface coating because the reflecting layer needs to be only a few hundred Å thick from the optical point of view. In crystal diffraction, the perfect-crystal layer too only needs to be several extinction distances thick, that is several tens of μm thick, but it must be ideally perfect. Such perfect epitaxy between dissimilar materials is simply not possible in practice so that the monochromator must be a single perfect crystal.

To *solve* the crystal thermal load problem, two solutions have been explored: to use different materials chosen for their thermal and mechanical properties (Bilderback, 1986; Freund, 1995) or to adapt the crystal shape so as to compensate for the thermal deformation (Berman & Hart, 1991; Quintana *et al.*, 1995; Schulte-Schrepping *et al.*, 1997). Compensation of the thermal deformation of surface figures has also been applied adaptively for mirrors (Susini *et al.*, 1991).

Two different materials have emerged that offer excellent solutions to the high-heat-load monochromator problem: silicon used at about 120 K where the thermal-expansion coefficient is zero (Bilderback, 1986) and the thermal conductivity is almost ten times higher than at room temperature; and diamond used at room temperature (Freund, 1995). From the point of view of thermal design, the figure of merit for a mirror or monochromator material is just k/α. Materials with high thermal conductivity and low thermal expansion are clearly advantageous in X-ray optics. However, the power absorbed in thin slices is determined by the X-ray linear absorption coefficient μ, but the meaning of the description 'thin' is strongly dependent on the X-ray

Table 4. *Figures of merit for mirror and monochromator materials*

	Diamond	Silicon	Germanium
μ (10 keV) (mm^{-1})	0.74	7.5	18.5
k at 300 K (W m^{-1} K^{-1})	3500	160	64
k at 77 K (W m^{-1} K^{-1})		1330	360
α/C at 300 K	0.8×10^{-6}	2.33×10^{-6}	5.8×10^{-6}
α/C at 77 K		-0.5×10^{-6}	1.4×10^{-6}
k/α (W m^{-1} at 300 K)	4.38×10^9	68.7×10^6	11.0×10^6
k/α (W m^{-1} at 77 K)		2.66×10^9	257×10^6
k/αμ (W at 300 K)	5.9×10^6	9.16×10^3	0.60×10^3
k/αμ (W at 77 K)		0.36×10^6	13.9×10^3

energy. Silicon wafers are almost totally absorbing at 5 keV but almost totally transparent at 100 keV so that the incorporation of X-ray parameters such as absorption or scattering power into X-ray-optical figures of merit is complicated in practice. Some values are given in Table 4.

The figures of merit show the advantages of cryogenically cooled silicon and diamond over other possible materials. The figure of merit $k/\alpha\mu$, which includes the X-ray absorption coefficient μ, is particularly relevant in the Laue case of transmission where the absorbed power increases with μ whereas the value of k/α is relevant to the Bragg case of reflection and to mirrors where the power is essentially totally absorbed. Freund (1995) has comprehensively reviewed diamond X-ray optics. Marot (1995) recently reviewed the progress of cryogenic cooling crystal designs that are now in routine use at third-generation synchrotron-radiation facilities, handling without compromise the high heat loads.

7. Future prospects

For crystal X-ray monochromators, three important materials, diamond, silicon and germanium, are readily available commercially. For mirrors and multilayers, important substrates that are readily available commercially are silicon, glass of several varieties, aluminium and Glidcop, all offered with a range of coating and multilayer film combinations. Mechanical engineering design and modeling can therefore be undertaken with confidence in both the X-ray optical and (thermo)mechanical performance of beamline components (SRI'97, 1998). Optical performance can be properly characterized using the DuMond (1937) diagram approach, *via* ray-tracing (*e.g.* the *SHADOW* program) (Lai & Cerrina, 1986) and phase-space methods (Hastings, 1977; Matsushita & Kaminaga, 1980*a,b*), which are capable of folding in source properties and optics distortion, and can therefore provide insight into the best match of beamline optics to a particular set of source characteristics. The final step, to incorporate deformed crystal dynamical theory (Takagi, 1962, 1968; Taupin, 1964; Authier & Malgrange, 1998)

into the design process, is under way. When these elements are fully integrated into future design strategies, it will be possible to create high performance with a level of confidence similar to that already achieved in visible light optics, even if source power and brightness continue to increase.

References

Authier, A. & Malgrange, C. (1998). *Acta Cryst.* A**54**, 806–819.

Batterman, B. W. (1962). *Appl. Phys. Lett.* **1**, 68–69.

Batterman, B. W. (1992). *Phys. Rev. B*, **45**, 12677–12681.

Belyakov, V. A. & Dmitrienko, V. E. (1991). *Sov. Phys. Usp.* **32**, 697–719.

Berman, L. E., Durbin, S. M. & Batterman, B. W. (1985). *Nucl. Instrum. Methods*, A**241**, 295–301.

Berman, L. E. & Hart, M. (1991). *Nucl. Instrum. Methods Phys. Res.* A**302**, 558–562.

Bilderback, D. H. (1986). *Nucl. Instrum. Methods Phys. Res.* A**246**, 434–436.

Bonse, U. & Hart, M. (1965). *Appl. Phys. Lett.* **7**, 238–240.

Bonse, U., Olthoff-Münter, K. & Rumpf, A. (1983). *J. Appl. Cryst.* **16**, 524–531.

Borrmann, G. (1941). *Phys. Z.* **42**, 157–162.

Borrmann, G. (1950). *Z. Phys.* **127**, 297–323.

Bragg, W. H. (1914). *Philos. Mag.* **27**, 881–899.

Bragg, W. H. (1915). *Philos. Trans. R. Soc. London Ser. A*, **215**, 253–274.

Brogren, G. & Adell, Ö. (1954). *Ark. Fys.* **8**, 401–410.

Brümmer, O., Höche, H. R. & Nieber, J. (1979). *Phys. Status Solidi A*, **53**, 565–570.

Campbell, H. N. (1951). *J. Appl. Phys.* **22**, 1139–1142.

Caticha, A. & Caticha-Ellis, S. (1982). *Phys. Rev. B*, **25**, 971–983.

Chandrasekaran, K. S. (1959). *Acta Cryst.* **12**, 916–945.

Cole, H., Chambers, F. W. & Wood, C. G. (1961). *J. Appl. Phys.* **32**, 1942–1945.

Compton, A. H. (1934). In *X-rays in Theory and Experiment*, edited by A. H. Compton and S. K. Allison. New Jersey: Van Nostrand Co.

Darwin, C. G. (1914a). *Philos. Mag.* **27**, 315–332.

Darwin, C. G. (1914b). *Philos. Mag.* **27**, 675–689.

Davis, B. & Stemple, W. (1921). *Phys. Rev.* **17**, 608–623.

Davis, B. & Stemple, W. (1922). *Phys. Rev.* **19**, 504–511.

Dorner, B., Burkel, E. & Peisl, J. (1986). *Nucl. Instrum. Methods*, A**246**, 450–451.

DuMond, J. W. M. (1937). *Phys. Rev.* **52**, 872–883.

Ehrenberg, W. & Mark, H. (1927). *Z. Phys.* **42**, 807–822.

Ewald, P. P. (1917). *Ann. Phys. (Leipzig)*, **54**, 519–597.

Ewald, P. P. (1950). In *Fifty Years of X-ray Diffraction*. Utrecht: N. V. A. Oosthoek.

Freund, A. K. (1995). *Opt. Eng.* **34**, 432–440.

Graeff, A. W. & Materlik, G. (1982). *Nucl. Instrum. Methods*, **195**, 97–103.

Hart, M. (1978). *Philos. Mag.* B**38**, 41–56.

Hart, M. & Rodrigues, A. R. D. (1978). *J. Appl. Cryst.* **11**, 248–253.

Hart, M. & Rodrigues, A. R. D. (1979). *Philos. Mag.* **40**, 149–157.

Hart, M., Rodrigues, A. R. D. & Siddons, D. P. (1984). *Acta Cryst.* A**40**, 502–507.

Hastings, J. B. (1977). *J. Appl. Phys.* **48**, 1576–1584.

Hirano, K., Ishikawa, T., Koreeda, S., Fuchigami, K., Kanzaki, K. & Kikuta, S. (1992). *Jpn. J. Appl. Phys.* **31**, L1209–L1211.

Hirano, K., Izumi, K., Ishikawa, T., Annaka, S. & Kikuta, S. (1991). *Jpn. J. Appl. Phys.* **30**, L407–L410.

Hirsch, P. B. (1952). *Acta Cryst.* 5, 176–184.

Ishikawa, T., Yoda, Y., Izumi, K., Suzuki, C. K., Zhang, X. W., Ando, M. & Kikuta, S. (1992). *Rev. Sci. Instrum.* **63**, 1015–1018.

James, R. W. (1948). *The Optical Principles of the Diffraction of X-rays.* London: Bell and Sons.

Knowles, J. W. (1956). *Acta Cryst.* **9**, 61–69.

Kohler, M. (1933). *Ann. Phys. (Leipzig)*, **18**, 265–287.

Kohra, K. & Matsushita, T. (1972). *Z. Naturforsch. Teil A*, **27**, 484–487.

Lai, B. & Cerrina, F. (1986). *Nucl. Instrum. Methods*, A**246**, 337–341.

Laue, M. von (1949). *Acta Cryst.* **2**, 106–113.

Marot, G. (1995). *Opt. Eng.* **34**, 426–431.

Matsushita, T. & Hashizume, H. (1983). *Handbook of Synchrotron Radiation*, Vol. 1, edited by E. E. Koch, pp. 261–314. Amsterdam: North-Holland.

Matsushita, T. & Kaminaga, U. (1980a). *J. Appl. Cryst.* **13**, 465–471.

Matsushita, T. & Kaminaga, U. (1980b). *J. Appl. Cryst.* **13**, 472–478.

Mills, D. M. (1987). *Phys. Rev. B*, **36**, 6178–6181.

Prins, J. A. (1930). *Z. Phys.* **63**, 477–493.

Quintana, J. P., Hart, M., Bilderback, D., Henderson, C., Richter, D., Setterson, T., White, J., Hausermann, D., Krumrey, M. & Schulte-Schrepping, H. (1995). *J. Synchrotron Rad.* **2**, 1–5.

Ramachandran, G. N. (1948). *Acta Cryst.* **1**, 155–156.

Renninger, M. (1934). *Z. Kristallogr.* **89**, 344–374.

Schulte-Schrepping, H., Heuer, J. & Hukelmann, B. (1997). *J. Synchrotron Rad.* **5**, 682–684.

Schwarz, G. & Rogosa, L. (1954). *Phys. Rev.* **95**, 950–953.

Siddons, D. P., Hastings, J. B., Faigel, G., Grover, J. R., Haustein, P. E. & Berman, L. E. (1989). *Rev. Sci. Instrum.* **60**, 1649–1654.

Skalicky, P. & Malgrange, C. (1972). *Acta Cryst.* A**28**, 501–507.

Sparks, C. J., Borie, B. S. & Hastings, J. B. (1980). *Nucl. Instrum. Methods*, **172**, 237–242.

SRI'91 (1992). *Rev. Sci. Instrum.* **63**, 283–1629.

SRI'94 (1995). *Rev. Sci. Instrum.* **66**, 1271–2390.

SRI'97 (1998). *J. Synchrotron Rad.* **5**, 133–1186.

Stojanoff, V., Hämäläinen, K., Siddons, D. P., Hastings, J. B., Berman, L. E., Cramer, S. & Smith, G. (1992). *Rev. Sci. Instrum.* **63**, 1125–1127.

Susini, J., Förstner, G., Zhang, L., Boyer, C. & Ravelet, R. (1991). *Rev. Sci. Instrum.* **63**, 423–427.

Takagi, S. (1962). *Acta Cryst.* **15**, 1311–1312.

Takagi, S. (1968). *J. Phys. Soc. Jpn.* **26**, 1239–1253.

Taupin, D. (1964). *Bull. Soc. Fr. Minéral. Cristallogr.* **87**, 469–511.

Underwood, J. H. & Barbee, T. W. (1981). *Appl. Opt.* **20**, 3027–3034.

Zachariasen, W. H. (1945). *Theory of X-ray Diffraction in Crystals.* New York: Wiley.

Ziegler, E. (1995). *Opt. Eng.* **34**, 445–452.